

Effect of Nb Content on Mechanical Behavior and Structural Properties of W/(Zr₅₅Cu₃₀Al₁₀Ni₅)_{100-x}Nb_x Composite



MORTEZA MAHMOODAN, REZA GHOLAMIPOUR, SHAMSEDDIN MIRDAMADI, and SAID NATEGH

In the present study, (Zr₅₅Cu₃₀Al₁₀Ni₅)_{100-x}Nb_(x=0,1,2,3) bulk metallic glass matrix/tungsten wire composites were fabricated by infiltration process. Structural studies were investigated by scanning electron microscopy and X-ray diffraction method. Also, mechanical behaviors of the materials were analyzed using quasi-static compressive tests. Results indicated that the best mechanical properties *i.e.*, 2105 MPa compressive ultimate strength and 28 pct plastic strain before failure, were achieved in the composite sample with $X = 2$. It was also found that adding Nb to the matrix modified interface structure in W fiber/(Zr₅₅Cu₃₀Al₁₀Ni₅)₉₈Nb₂ since the stable diffusion band formation acts as a functionally graded layer. Finally, the observation of multiple shear bands formation in the matrix could confirm the excellent plastic deformation behavior of the composite.

DOI: 10.1007/s11661-017-4003-3

© The Minerals, Metals & Materials Society and ASM International 2017

I. INTRODUCTION

MOST monolithic bulk metallic glasses (BMGs) tend to form localized shear band and fail catastrophically upon yielding in compression test, resulting in low plasticity. In fact, these glasses usually exhibit very limited plasticity before fracture.^[1-5] In order to overcome this problem for the purpose of achieving an extended ductility, fabrication of BMG composites has been practiced.^[6-8] Several studies have focused on Zr-based BMGs matrix composites because of their high glass-forming abilities and mechanical properties. Furthermore, Zr-based BMG matrix composites with various reinforcements—fibers, particles or *in situ* formed phases—have been developed to prevent localized shear strain leading to the propagation of multiple shear bands and ductility improvement.^[9-16] However, the ductility improvement in W/Zr BMG matrix was paid less attention in the previous studies. Wang *et al.*^[17] reported 13.5 pct plastic strain in W/Zr₄₇Ti₁₃Cu₁₁Ni₁₀Be₁₆Nb₃ BMG matrix composite with Nb addition in 70 pct tungsten volume fraction. In addition, Qiu *et al.*^[18] achieved 13 pct plastic strain in W/(Zr₅₅Al₁₀Ni₅Cu₃₀)_{98.5}Si_{1.5} BMG matrix composite in 68 pct tungsten volume fraction.

Furthermore, during melt infiltration process, diffusion band is established in the interface of W/Zr BMG

composite, *i.e.*, interdiffusion between melt and tungsten fiber. When a liquid alloy spreads on a tungsten fiber, interdiffusion may result in partial dissolution of the tungsten fiber, resulting in the formation of crystalline phases. During the change in infiltration parameters *e.g.*, time and temperature, diffusion band is converted into reaction layer and convection of particles.^[2,19] The formation of reaction layer and convection of particles in W/BMG composite interface reduce mechanical properties of the composites prepared by infiltration.^[16,17,19,20] It seems that some refractory elements such as Nb and Ta can reduce the interface interaction of W/Zr BMG matrix composite. Some studies concluded that the interfaces of W/BMG composites prepared by melt infiltration are modified by minor Nb addition.^[16,17,20]

The present research aimed to systematically study the effect of Nb content in BMGs on mechanical (especially ductility) and structural properties of W/(Zr₅₅Cu₃₀Al₁₀Ni₅)_{100-x}Nb_x BMG matrix composite.

II. MATERIALS AND METHODS

Ingots of (Zr₅₅Cu₃₀Al₁₀Ni₅)_{100-x}Nb_(x=0,1,2,3) (at. pct) were prepared by arc melting high-purity elements in Ti-gettered and Ar atmosphere in a water-cooled cooper crucible. Zr and Nb elements were first melted together and then other elements were added to the Nb-Zr ingot and remelted several times to form a homogeneous alloy. In the next step, the prepared melted alloy was cast into a water-cooled copper mold to make BMG rods with 4-mm diameters. A tungsten wire of 1-mm diameter was straightened and cut into 50-mm lengths and cleaned in an ultrasonic bath of acetone and

MORTEZA MAHMOODAN, SHAMSEDDIN MIRDAMADI, and SAID NATEGH are with the Department of Materials Engineering, Science and Research Branch, Islamic Azad University, Tehran 1477893855, Iran. REZA GHOLAMIPOUR is with the Institute of Advanced Materials and Renewable Energies, Iranian Research Organization for Science and Technology, Tehran 3353136846, Iran. Contact e-mail: rgholamipour@gmail.com

Manuscript submitted February 2, 2016.

Article published online February 15, 2017

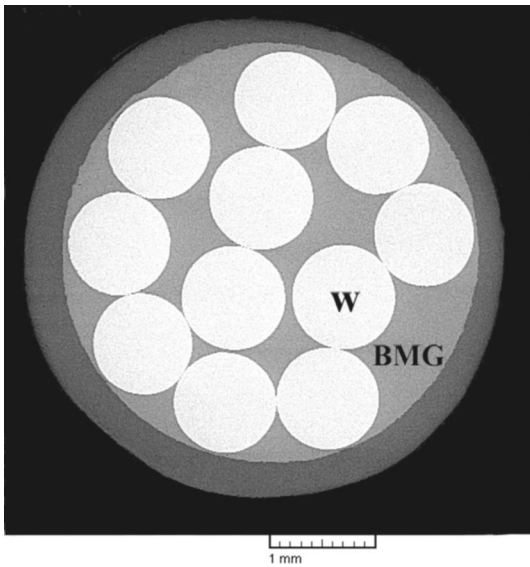


Fig. 1—Cross section of the as-produced composite.

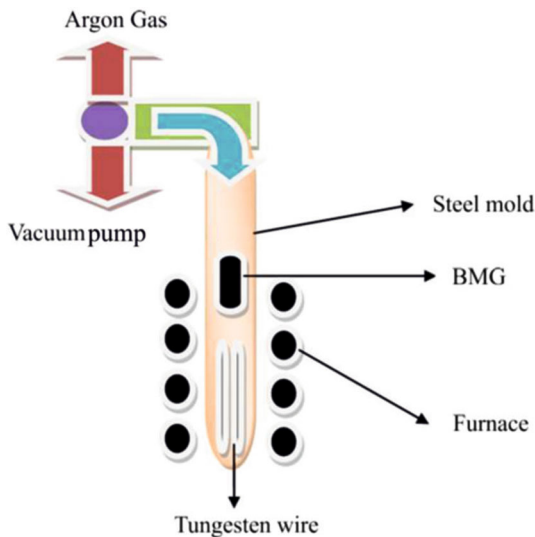


Fig. 2—Schematic infiltration set-up during melting process.

ethanol. The tungsten wires were placed at the bottom of sealed 4-mm ID stainless steel tubes (304) (Figure 1).

The volume fraction of tungsten wires was 70 pct. The assembly of the tubes was washed by repeated evacuation (up to 10^{-5} mbar) and by purging high-purity Ar gas several times followed by heating at various temperatures of 1198 K, 1223 K, and 1248 K (925 °C, 950 °C, and 975 °C) above the liquidus temperature of the BMG in an electrical furnace. The composite samples were then kept for 15 minutes under a 3.5 bar Ar pressure before they were quenched in water. The liquidus temperature of $(Zr_{55}Cu_{30}Al_{10}Ni_5)$ alloy was reported to be 1163 K (890 °C) in Reference 21. The infiltration temperatures of 308 K to 358 K (35 °C to 85 °C) above the liquidus temperature were selected as appropriate. Infiltration time was selected in a range of 5 to 20 minutes according to the previous studies.^[14–16,19]

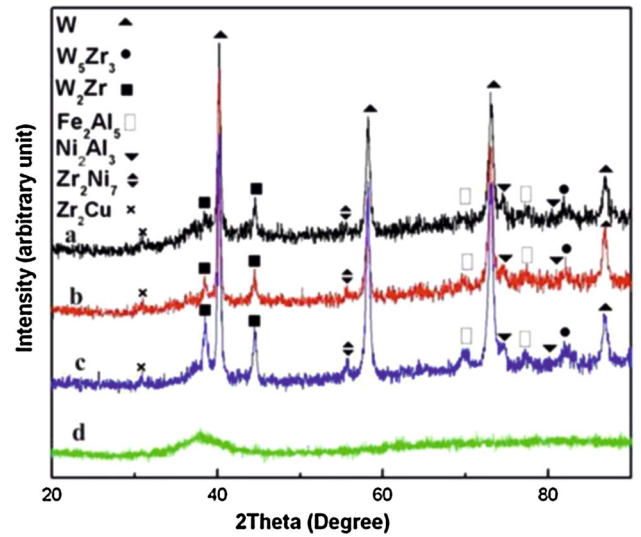


Fig. 3—XRD patterns of the infiltrated $W/(Zr_{55}Cu_{30}Al_{10}Ni_5)$ composite samples at different temperatures, (a) 1198 K (925 °C), (b) 1223 K (950 °C), (c) 1248 K (975 °C) for 15 min and (d) as-cast $(Zr_{55}Cu_{30}Al_{10}Ni_5)$ BMG.

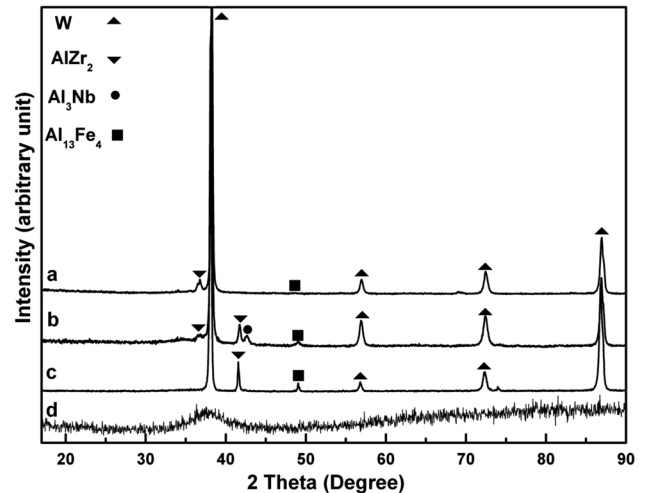


Fig. 4—XRD patterns of the infiltrated $W/(Zr_{55}Cu_{30}Al_{10}Ni_5)_{100-x}Nb_{(x=1,2,3)}$ composites at 1223 K (950 °C), (a) $X = 2$, (b) $X = 3$, (c) $X = 1$, for 15 min, and (d) as-cast $(Zr_{55}Cu_{30}Al_{10}Ni_5)_{98}Nb_2$ BMG.

However, the highest bulk density of the composites samples determined by Archimedes test was achieved by 15-minutes infiltration time. Figure 2 illustrates the schematic infiltration set-up.

In order to prepare quasi-static compression test samples, the composite specimens were cut by a low-speed saw. Mechanical properties were measured with a SANTAM (STM250) testing machine in which the strain rate set at $10^{-4} s^{-1}$. The gauge dimension of specimens was 4 mm in diameter and 8 mm in height for the compressive test. The attached steel mold around the specimens was removed before compressive testing. In order to understand the fracture behavior of the composite samples during plastic deformation, some samples whose lateral surfaces were partially polished

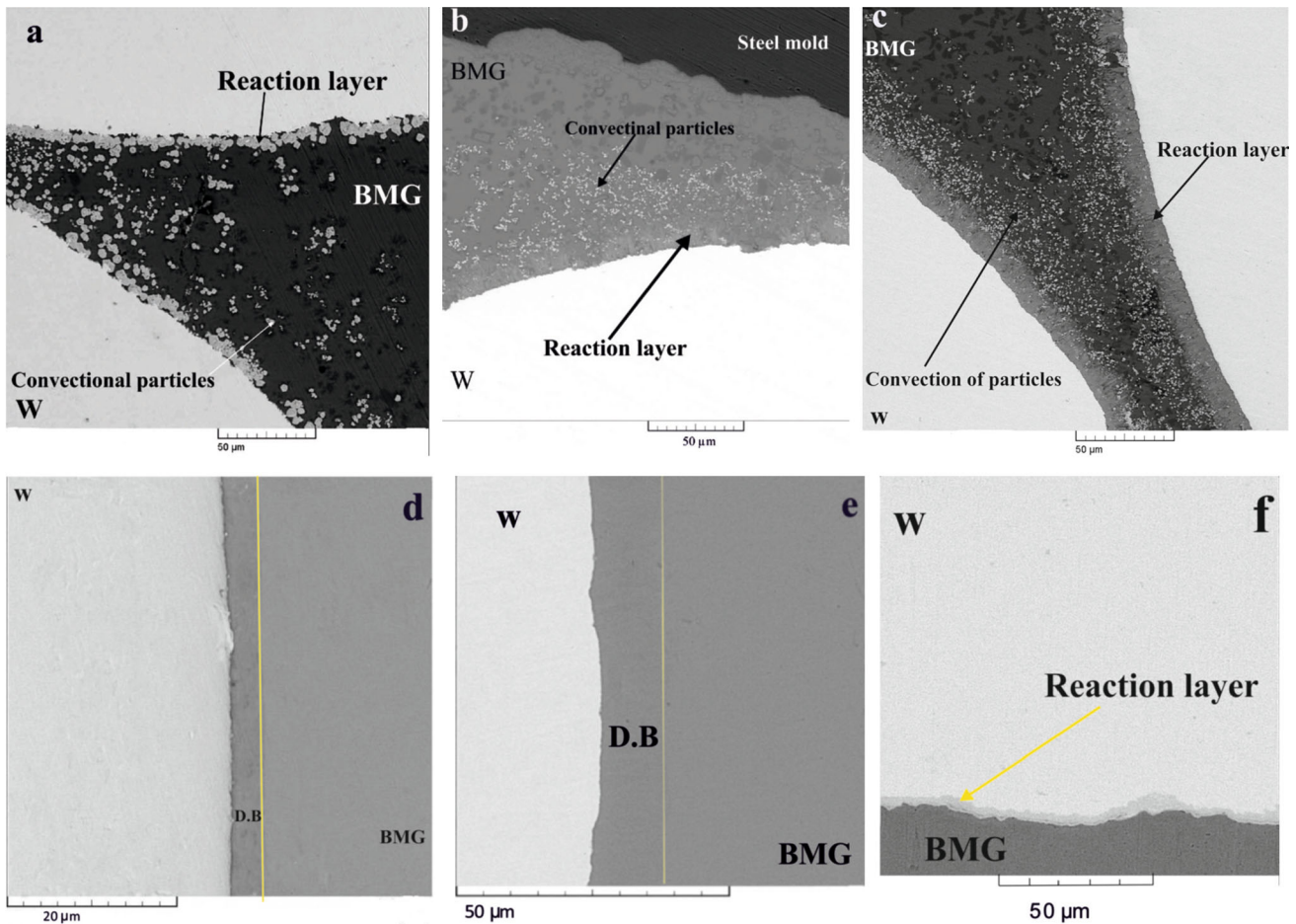


Fig. 5—The backscattered SEM micrographs of infiltrated $W/(Zr_{55}Cu_{30}Al_{10}Ni_5)_{100-x}Nb_{(x=0,1,2,3)}$ composites at different temperatures for 15 min. (a, b, c) $X = 0$, at 1198 K, 1223 K, 1248 K (925 °C, 950 °C, and 975 °C), respectively. (d) $X = 1$, (e) $X = 2$, and (f) $X = 3$, at 1223 K (950 °C).

were unloaded in three points: (i) after yield point in the composite sample with $X = 0$ and after 6 pct plastic deformation in the composite sample with $X = 2$; (ii) after 14 pct plastic deformation in the composite sample with $X = 2$ and the fracture point in the composite sample with $X = 0$; and (iii) the fracture point in the composite sample with $X = 2$. Microhardness of the specimen was measured by a hardness indenter with a load of 50 gf. The phase characterization and microstructural observations were carried out by X-ray diffraction (XRD) with Cu $K\alpha$ radiation and Field Emission Scanning Electron Microscopy (FESEM).

III. RESULTS AND DISCUSSIONS

Figure 3 indicates the XRD diffraction patterns of the as-cast $(Zr_{55}Cu_{30}Al_{10}Ni_5)_{100-x}Nb_{(x=0)}$ BMG and the infiltrated $W/(Zr_{55}Cu_{30}Al_{10}Ni_5)_{100-x}Nb_{(x=0)}$ composite samples at different temperatures for 15 minutes.

According to Figure 3, the Nb-free composite samples show some diffraction peaks from tungsten wires and some other crystalline phases originated by amorphous phase. The intensity of some peaks (such as W_2Zr peak in a range of $2\theta = 38.52$ deg) increased distinctly

with an increase in the infiltration temperature [from 1198 K to 1248 K (925 °C to 975 °C)]. The XRD diffraction patterns of the as-cast $(Zr_{55}Cu_{30}Al_{10}Ni_5)_{100-x}Nb_{(x=2)}$ BMG and the infiltrated $W/(Zr_{55}Cu_{30}Al_{10}Ni_5)_{100-x}Nb_{(x=1,2,3)}$ composite samples at 1223 K (950 °C) for 15 minutes are illustrated in Figure 4.

As it is evident from Figure 4, lack of the main intermetallic phases (W_2Zr and W_5Zr_3) in the composite samples is clearly observable. According to W-Zr phase diagram, the peritectic reaction product is W_2Zr ; however, W_5Zr_3 , as a metastable phase, should be transformed into the stable W_2Zr phase.^[15,17] As a result of an interaction between Al in the matrix and Fe in the steel tube during infiltration process, some other intermetallic crystalline phases such as (Fe_2Al) and $(Al_{13}Fe_4)$ can be established. As shown in Figure 4, the crystalline phase of (Al_3Nb) was formed in the composite sample with $X = 3$. Furthermore, an increase in the infiltration temperature led to an increase in the intensity of Al_3Nb peaks. This phase was not observed in the XRD pattern of the composite samples with $X = 1$ and $X = 2$. The excess Nb precipitation was probably converted into the new composition crystalline phase (Al_3Nb) in the matrix and an interface of the composite sample with $X = 3$.

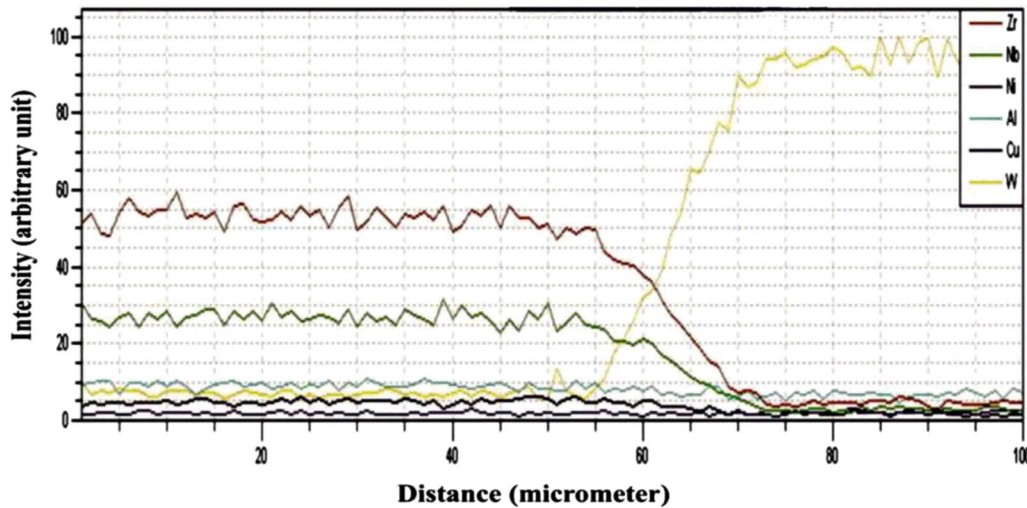
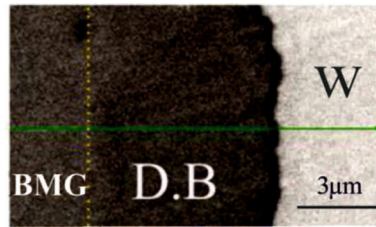


Fig. 6—Energy Dispersive Spectroscopy (EDS) line scan of diffusion band for the W/(Zr₅₅Cu₃₀Al₁₀Ni₅)₉₈Nb₂ composite sample infiltrated at 1223 K (950 °C) for 15 min.

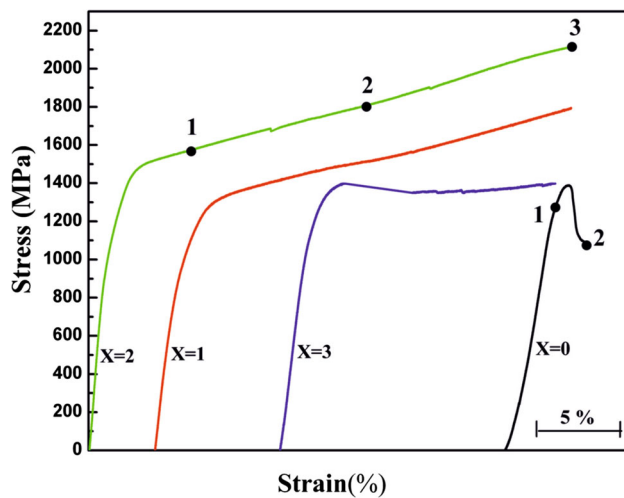


Fig. 7—The quasi-static stress–strain curves of the infiltrated W/(Zr₅₅Cu₃₀Al₁₀Ni₅)_{100-x}Nb_(x=0,1,2,3) composite samples at 1223 K (950 °C) for 15 min (point 1) after yield point in the composite sample with X = 0 and after 6 pct plastic deformation in the composite sample with X = 2, point (2) after 14 pct plastic deformation in the composite sample with X = 2 and the fracture point in the composite sample with X = 0, point (3) the fracture point in the composite sample with X = 2).

Moreover, the appropriate affinity between Al and Nb ($\Delta H_{\text{mixing}} = -84 \text{ kJ/mol}$)^[22] led to the formation of the crystalline phase (Al₃Nb) in the composite sample with X = 3 during the infiltration process.

Figure 5 illustrates the backscattered SEM micrographs of W/(Zr₅₅Cu₃₀Al₁₀Ni₅)_{100-x}Nb_(x=0,1,2,3)

Table I. The Quasi-static Compressive Test Results of Infiltrated W/(Zr₅₅Cu₃₀Al₁₀Ni₅)_{100-x}Nb_(x=0,1,2,3) Composites at 1223 K (950 °C) for 15 min

Composite Sample	σ_c (MPa)	ϵ_c (pct)
X = 0	1384 ± 38	2.5 ± 1
X = 1	1788 ± 42	25 ± 1.5
X = 2	2105 ± 35	28 ± 2
X = 3	1294 ± 48	14 ± 1

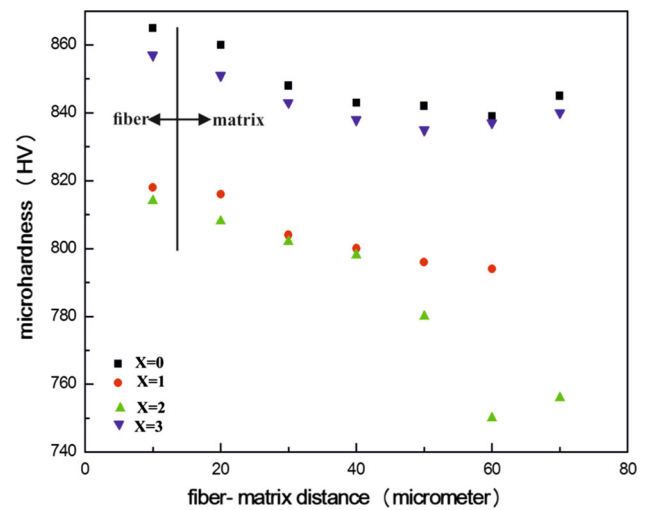


Fig. 8—The microhardness scans of fiber toward matrix in W/(Zr₅₅Cu₃₀Al₁₀Ni₅)_{100-x}Nb_(x=0,1,2,3) composite samples infiltrated at 1223 K (950 °C) for 15 min.

composite samples infiltrated at different temperatures for 15 minutes. According to this figure, the thickness of reaction layer in the composite sample with $X = 0$ increased (from 5 to about 10 μm) with the increase in the infiltration temperature from 1198 K to 1248 K (925 °C to 975 °C) due to the conversion of reaction layer into convection particles near interface in the infiltrated composite sample at 1248 K (975 °C). The results are congruent with Khademian *et al.*^[19] study in which they concluded that there was an increase in the thickness of the convection particles when the infiltration temperature rose from 1223 K to 1273 K (950 °C to 1000 °C) in W/Zr₆₅Cu_{17.5}Ni₁₀Al_{7.5} BMG matrix composites after 20 minutes. According to Figure 3, increasing the infiltration temperature from 1198 K to 1248 K (925 °C to 975 °C) results in enhanced intensity of W₂Zr phase. Generally, during melt infiltration, the matrix elements are diffused in the tungsten wires forming the reaction layers by an increase in infiltration temperature. Due to the erosion of tungsten wire in this process, the strength of tungsten grain boundary drops and leads to the formation of rich tungsten particles in the matrix.^[19] Among the matrix elements, Zr is severely reacted with tungsten, thanks to high affinity among them,^[22] and the W₂Zr intermetallic crystalline phase is established in the interface or near the interface in the matrix of composite. EDS results proved that the white particles' composition in Figures 5(a) through (c) is rich in Zr and W elements (not shown here). Therefore, according to the results of XRD (Figure 3) and EDS, the white particles formed in (or near) the interface are W₂Zr compound.

As illustrated in Figures 5(d) through (f), the diffusion band (DB) is stable in the composite samples with $X = 1$ and $X = 2$ with the thickness of about 4 and 12 μm , respectively. However, in the composite sample ($X = 3$), the diffusion band is not stable and is converted into a reaction layer. According to XRD the findings (Figure 4), formation of the Al₃Nb crystalline phase in the matrix and the interface of the composite sample with $X = 3$ during the infiltration process are probably the main reason for the diffusion band instability in this composite sample.

The Nb alloy element because of the strong affinity between W and Nb ($\Delta H_{\text{mixing}} = -34 \text{ kJ/mol}$) prevents the interaction between W and Zr at the interface and decreases the diffusion coefficient of Zr in the melted matrix alloy to the solid W fibers.^[17,20,22–25] Li *et al.*^[26] by calculating the interaction energy of some elements and W reported that Nb is preferred to segregate on the W substrate surface in (Zr_{40.08}Ti_{13.30}Cu_{11.84}Ni_{10.07}Be_{24.71})₉₅Nb₅ alloy system resulting in an effective suppression of W-Zr reaction in the composite interface. Figure 6 illustrates the energy dispersive spectroscopy (EDS) line scan from the matrix to fiber of the composite sample with $X = 2$.

According to Figure 6, there is a gradual intensity change in tungsten from 100 to 0 at. pct in the DB. In other words, this kind of DB performs as a functionally graded layer leading to the improvement of crack propagation resistance of a composite.^[27]

Figure 7 shows the quasi-static stress–strain curves of the infiltrated W/(Zr₅₅Cu₃₀Al₁₀Ni₅)_{100-x}Nb_x($x=0,1,2,3$) composite samples at 1223 K (950 °C) for 15 minutes. The quantitative results of the stress–strain curves (Figure 7) are summarized in Table I.

The composite sample with $X = 2$ has the best mechanical properties including (plastic strain and compressive strength) while the lowest plastic strain belongs to the composite sample with $X = 0$. As it is evident from Table I, the amount of plastic strain in the composite sample with $X = 2$ achieved 28 pct, showing an extended ductility in comparison with other research studies.^[17,20,23,24] The small difference in ductility between the composite sample with $X = 2$ and $X = 1$ is due to the same structure of the BMG matrix of these composites during infiltration process (Figure 4).

According to Figure 5, the thickness of diffusion band in the composite sample with $X = 1$ is less than that of $X = 2$. As it was already mentioned, the DB is a functionally graded layer. In fact, the lower Nb content in the matrix, the lower thickness of DB, and the higher concentration gradient of tungsten are directly dependent on each other. Since the higher gradient of interface causes the materials to have a higher sensitivity to crack formation and propagation,^[27] there should be a decrease in the strength of the composite sample with $X = 1$ rather than the sample with $X = 2$. Further research is needed for detailed understanding of the issue.

The existence of crystalline phases, especially W₂Zr and W₅Zr₃ forming in or near the interface (Figures 5(a) through (c)) as the crack nucleation sites, justifies the lack of plastic strain in the composite sample with $X = 0$. In previous studies, some researchers came to this conclusion that reactions at the interface are inevitable in Zr-based BMG matrix composite during casting and excessive reaction debilitates reinforcements leading to the loss of mechanical properties of the composite sample.^[17,20]

As illustrated in Table I, the mechanical properties of the composite sample with $X = 3$ decreased in comparison with the composite samples with $X = 1$ and $X = 2$. The main reason might be attributed to the instability of diffusion band (Figure 5) or a decrease in the interface strength due to the formation of (Al₃Nb) crystalline phase in the matrix or the interface of the composite sample with $X = 3$, confirmed by XRD pattern (Figure 4) and SEM observation (Figure 5).

The calculated buckling stress for tungsten wire is estimated from Eq. [1]^[11]:

$$\sigma_{\text{buckling}} = \frac{\pi^2 E_f d_f^2}{16 l_f^2}, \quad [1]$$

where E_f is the Young's modulus of the fiber (~410 GPa), d_f is the diameter of the fiber (1 mm), and l_f is the length of the fiber (8 mm). According to Eq. [1], buckling stress is calculated as 1601 MPa.

Dragoi *et al.*^[28] simulated the thermal residual stress in fiber/metallic glass composite and reported that the thermal residual stress in longitudinal and transverse direction in the BMG matrix is under tensile stress while W fiber is under compressive stress. Furthermore, Wang

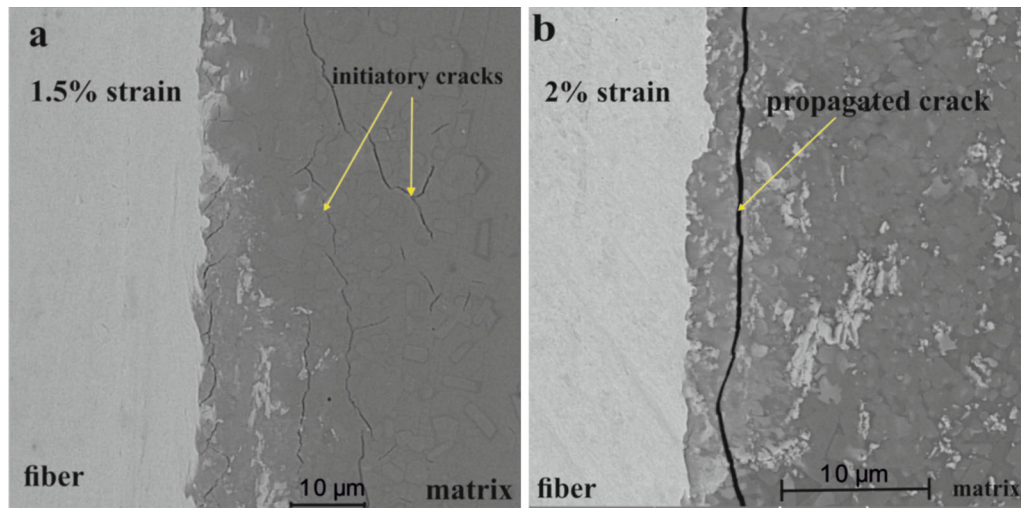


Fig. 9—The backscattered SEM micrographs in matrix and fiber at different stages of quasi-static compressive test in the infiltrated W/ $(\text{Zr}_{55}\text{Cu}_{30}\text{Al}_{10}\text{Ni}_5)_{100-x}\text{Nb}_{(x=0)}$ composite at 1223 K (950 °C) for 15 min, according to the two points in Fig. 7, (a) point (1), (b) point (2).

et al.^[11] found the same condition in $\text{Zr}_{41.25}\text{Ti}_{13.75}\text{Ni}_{10}\text{Cu}_{12.5}\text{Be}_{22.5}$ bulk metallic glass composite reinforced with tungsten wires and reported that the tensile frozen-in stresses is doubled, compared to the compressive frozen-in stresses in the longitudinal direction. Hence, during the plastic deformation, there are three stresses on the tungsten wires, the longitudinal external stress, the residual stress (established in the sample after quenching), and the buckling stress. After the wires are buckled, the BMG matrix should be squeezed to relieve stress and weaken lateral support for the next layer of wires. In contrast, the wires close to the center of the W-BMG composite are fully supported by the BMG matrix and require much higher buckling.^[11] Accordingly, the work hardening takes place in the composite samples with $X = 1$ and $X = 2$ when there is probably an increase in compressive stresses in central tungsten wires as well as in dislocation density.

Considering the results in Figure 7, the mechanical behavior of the composite samples is different after these phenomena. In the composite sample with $X = 0$ because of the formation of reaction layer and convection particles as crack nucleation sites, work hardening is not observed and softening happens instead. In the composite sample with $X = 3$ due to the formation of reaction layer (Figure 5), the work hardening slope markedly decreases, resulting in the diffusion band instability.

The microhardness scans of the infiltrated W/ $(\text{Zr}_{55}\text{Cu}_{30}\text{Al}_{10}\text{Ni}_5)_{100-x}\text{Nb}_{(x=0,1,2,3)}$ composite samples from fiber toward matrix are shown in Figure 8. It is evident that the composite sample with $X = 0$ has the highest average microhardness while the composite with $X = 2$ has the lowest one among the composite samples, confirming the mechanical and structural properties of the samples. On the other hand, by considering the results in Figures 3 and 7 and their comparison with Figure 8, the existence of the hard crystalline phases leads to an increase in the average hardness and a

decrease in the ductility in the composite sample with $X = 0$.

The results are consistent with those reported by Devinder and Qiu on composite samples with amorphous matrix, who confirmed that an increase in plasticity leads to a decrease in matrix hardness.^[12,29]

The microstructural features of the composite samples during the quasi-static compressive test are shown in Figures 9 and 10.

By looking at Figures 9, the backscattered SEM micrographs of the BMG matrix and infiltrated W/ $(\text{Zr}_{55}\text{Cu}_{30}\text{Al}_{10}\text{Ni}_5)_{100-x}\text{Nb}_{(x=0)}$ composite sample were obtained according to point 1 and 2 in Figure 7. It is illustrated from Figure 9(a) that the microcracks are nucleated in the matrix during the plastic deformation in the composite sample with $X = 0$ propagated and moved near the interface of W/BMG composite with an increase in external loading (Figure 9(b)). The main crystalline intermetallic phases (W_2Zr and W_5Zr_3) in the matrix near the interface of the composite sample with $X = 0$ during the infiltration are potential sites for the nucleation of cracks in the composite matrix.

The propagation and branching of the shear bands at the different stages of deformation as it is observed from Figure 10 lead to an increase in the plastic strain. The result of this study can be regarded as a support for the findings of researchers^[17,23,29–32] who also reported that the plastic deformation of the composite directly depends on the formation and propagation of shear bands. Also, Lee *et al.*^[33] concluded that the stress field near the second phase can be served as an effective barrier to the direct propagation of the shear bands, leading to shear band branching in various Cu-Zr including monolithic amorphous alloys.

Furthermore, as shown in Figure 10(c), the diffusion band in the composite sample with $X = 2$ plays a pivotal role in branching shear bands in such a way that the shear bands are stopped and branched in the matrix after interaction with the diffusion band. As it was

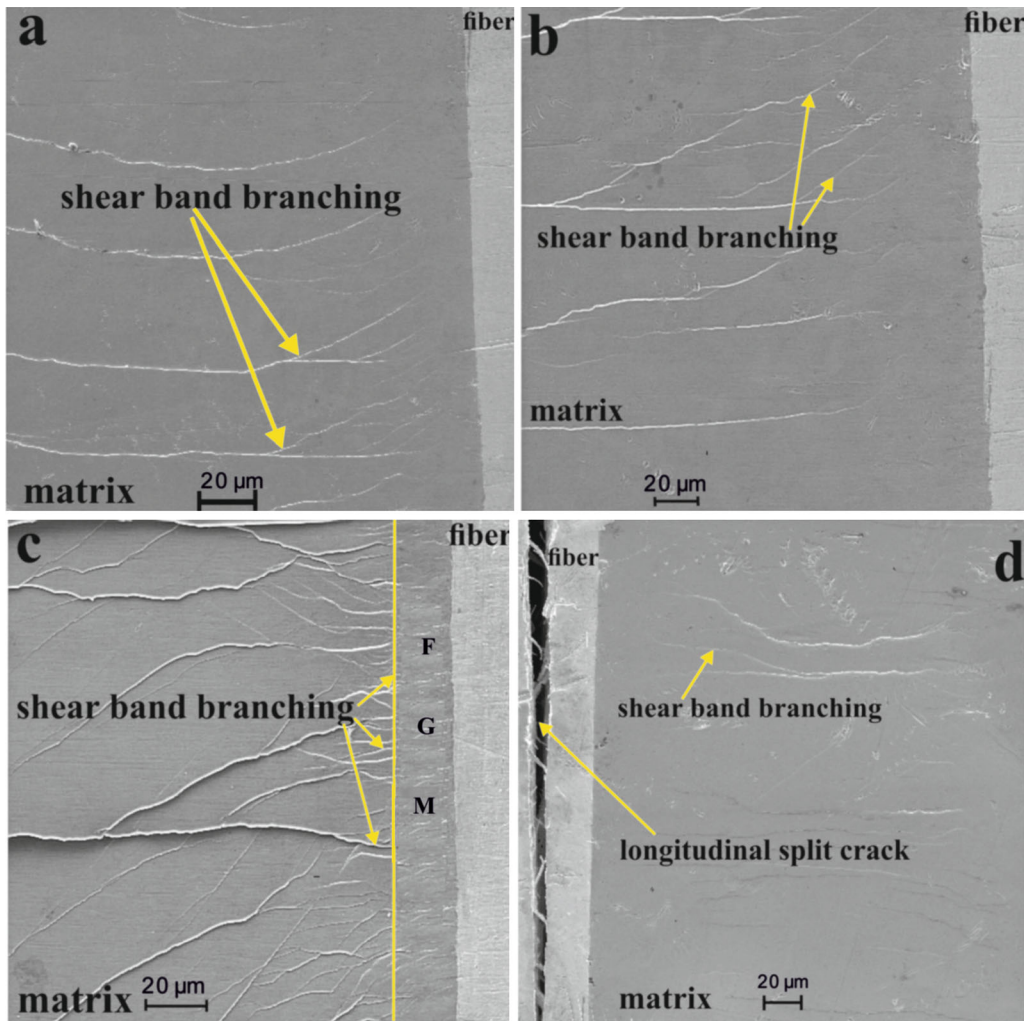


Fig. 10—The backscattered SEM micrographs in matrix and fiber at different stages of quasi-static compressive test in the infiltrated W/ $(Zr_{55}Cu_{30}Al_{10}Ni_5)_{98}Nb_2$ composite at 1223 K (950 °C) for 15 min, according to the three points in Fig. 7, (a) point (1), (b) point (2), (c, d) point (3), in which FGM represents the functionally graded material (layer).

already mentioned, the diffusion band acts as a functionally graded layer. Some researchers reported that the most important characteristic of functionally graded materials is the ability to inhibit crack propagation and reduce the driving force for crack growth, due to the lack of stress concentration resulting from the continuous microstructure change across the layer, compared with a sharp change in an interface.^[27,34–36] In other words, in the composite sample with $X = 2$, the tailored interface with a functionally graded layer triggers an appropriate distribution and stress transfer around the critical region of crack nucleation site (interface) leading to the improvement of the mechanical properties of the composite material.

On the contrary, in the composite sample with $X = 0$, due to an interaction of stored elastic energy and the stress field barrier near the crystalline phases, the shear bands are rapidly converted into shear cracks and accordingly, they cannot branch in the matrix, leading to a dramatic reduction in the composite ductility (Figure 9).

At the fracture point of the composite sample with $X = 2$, the longitudinal splitting fracture mode takes place within the tungsten fiber near the W/BMG interface region as it is shown in Figure 10(d). Chen *et al.*^[37] also indicated that the splitting fracture in tungsten fiber results from the transverse stress in buckled tungsten fiber during deformation in W/BMG composite with 70 pct tungsten volume fraction. In fact, a fracture of the composite sample with $X = 2$ occurred in the wires due to the high resistivity of diffusion band (as a functionally graded layer) against the crack formation, propagation in the matrix, and concentration of compressive stresses in the fibers.

IV. CONCLUSION

Results of the present study indicated that there is an optimum amount of Nb in the matrix ($X = 2$), which is able to minimize the hardness of intermetallic crystalline phases in the W/BMG composite interface significantly

and tailor the interface by a functionally graded layer, resulting in maximum mechanical properties. The optimum infiltration temperature and time in the composite production were 1223 K (950 °C) and 15 minutes, respectively, for the purpose of attaining the best mechanical properties, *i.e.*, 2105 MPa compressive ultimate strength and 28 pct plastic strain before failure.

REFERENCES

1. R.D. Conner, R.B. Dandliker, V. Scruggs, and W.L. Johnson: *Int. J. Impact Eng.*, 2000, vol. 24, pp. 435–44.
2. X. Hui, J. Yu, M. Wang, W. Dong, and G. Chen: *Intermetallics*, 2006, vol. 14, pp. 931–35.
3. D. Dargoi, E. Ustundag, B. Clausen, and M.A. Bourke: *Scripta Mater.*, 2001, vol. 45, pp. 245–52.
4. F. Abdeljawad, M. Fontus, and M. Haataja: *J. Appl. Phys.*, 2011, vol. 98, pp. 03190-1–3.
5. S.T. Deng and H. Diao: *Scripta Mater.*, 2011, vol. 64, pp. 85–88.
6. H. Li and K. Li: *Sci. Eng. A*, 2006, vol. 429, pp. 115–23.
7. J. Qiao and Y. Zhang: *Intermetallics*, 2011, vol. 19, pp. 149–53.
8. B.Y. Zhang, X. Chen, and S. Wang: *Mater. Lett.*, 2013, vol. 93, pp. 210–14.
9. H. Zhang, H. Li, and A.M. Wang: *Intermetallics*, 2009, vol. 17, pp. 1070–77.
10. G.Y. Sun and G. Chen: *Intermetallics*, 2007, vol. 15, pp. 632–34.
11. G. Wang, D.M. Chen, J. Shen, Zh. Stanchurski, Q.H. Qin, J.F. Sun, and B.D. Zhou: *J. Non-Cryst. Solids*, 2006, vol. 352, pp. 3872–78.
12. D. Singh and R.K. Mandal: *J. Alloy. Compd.*, 2011, vol. 509, pp. 8657–63.
13. L. Liu and Q. Chen: *Mater. Sci. Eng. A*, 2007, vol. 449, pp. 949–53.
14. Q.S. Zhang, H.F. Zhang, B.Z. Ding, and Z.Q. Hu: *Mater. Sci. Eng. A*, 2003, vol. 360, pp. 280–84.
15. K.Q. Qiu and Y.L. Ren: *J. Miner. Mater. Charact. Eng.*, 2004, vol. 3, pp. 91–98.
16. N. Khademian and R. Gholamipour: *Mater. Sci. Eng. A*, 2010, vol. 527, pp. 3079–84.
17. M.L. Wang, G.L. Chen, X. Hui, Y. Zhang, and Z.Y. Bai: *Intermetallics*, 2007, vol. 15, pp. 1309–15.
18. K.Q. Qiu, A.M. Wang, H.F. Zhang, B.Z. Ding, and Z.Q. Hu: *Intermetallics*, 2002, vol. 10, pp. 1283–88.
19. N. Khademian and R. Gholamipour: *J. Non-Cryst. Solids*, 2013, vol. 365, pp. 75–84.
20. J. Fei, C. Guang, W. Zhihua, C. Yang, C. Jialin, and C. Guoliang: *Rare. Metal. Mater. Eng.*, 2011, vol. 40, pp. 206–08.
21. A. Inoue and A. Takeuchi: *Acta Mater.*, 2011, vol. 59, pp. 2243–67.
22. A.R. Miedemax, F.R. Boerxx, and R. Boom: *Calphad*, 1977, vol. 1, pp. 341–59.
23. H. Wang, H.F. Zhang, and Z.Q. Hu: *Mater. Manuf. Process*, 2007, vol. 22, pp. 687–91.
24. H.G. Jeong, K. Hiraga, M. Mabuchi, and K. Higashi: *Acta Mater.*, 1998, vol. 46, pp. 6009–20.
25. M. Wang, H. Xioding, and G. Chen: *Matter. Sci. Forum.*, 2005, vols. 475–479, pp. 3389–92.
26. Z.K. Li, H.M. Fu, P.F. Sha, Z.W. Zhu, A.M. Wang, H. Li, H.W. Zhang, H.F. Zhang, and Z.Q. Hu: *Sci. Rep.*, 2015, vol. 5, pp. 8967–73.
27. S. Suresh and A. Mortensen: *In. Mater. Rev.*, 1997, vol. 42, pp. 85–116.
28. D. Dragoi, B. Clausen, and M.A. Bourke: *Scripta Mater.*, 2001, vol. 45, pp. 245–52.
29. K. Qiu, Z.Y. Suo, Y.L. Ren, and B. Yu: *J. Mater. Res.*, 2007, vol. 22, pp. 551–54.
30. J. Gu, S. Ni, X. Liao, and S. Guo: *Mater. Sci. Eng. A*, 2014, vol. 602, pp. 68–76.
31. C. Lia and S. Kou: *Prog. Nat. Sci. Mater. Int.*, 2012, vol. 22, pp. 21–25.
32. H.K. Lim, E.S. Park, and J.S. Park: *J. Mater. Sci.*, 2005, vol. 40, pp. 6127–30.
33. S. Lee, M. Huh, E. Fleury, and J. Lee: *Acta Mater.*, 2006, vol. 54, pp. 349–55.
34. W. Ruigang, P. Wei, J. Mengning, C. Jian, and L. Yongming: *Mater. Sci. Eng. B*, 2002, vol. 90, pp. 261–68.
35. C.S. Huang, O.G. Mcgee, and M.J. Chang: *Compos. Struct.*, 2011, vol. 93, pp. 1747–65.
36. L. Lu, M. Chekroun, O. Abraham, V. Maupin, and G. Villain: *NDT & E Int.*, 2011, vol. 44, pp. 169–77.
37. J.H. Chen, Y. Chen, M.Q. Jiang, X.W. Chen, H.M. Fu, H.F. Zhang, and L.H. Dal: *Metall. Mater. Trans. A*, 2014, vol. 45A, pp. 5397–5408.